P9.95 ENHANCED DETECTION CAPABILITY FOR DUAL POLARIZATION WEATHER RADAR

Reino Keränen[1]
Vaisala, Oyj., Helsinki, Finland

V. Chandrasekar
Colorado State University, Fort Collins CO, U.S.A.
University of Helsinki, Finland

1. INTRODUCTION

Most applications of dual-polarization weather radar favor using data at high signal-to-noise ratios, for improving echo identification and quantitative measurement. In fact, the transmitter power split ("3 dB loss") is seen as a trade-off in detection capability of the mode of simultaneous transmission and reception (STAR). It can be mitigated by combining moments to collect more signal, Ivic (2009, 2011). More signals can be arranged for by switching the operation into the H-only mode, or by adding transmitter power. All these have limited scopes.

We here explore dual-polarization as a method to improve detection of weak echo of precipitation. We recognize a mechanism of noise cancellation that is intrinsic in the off-diagonal element of the polarimetric signal covariance matrix. We study the degree of cancellation realized in finitely sampled rays. Combining these outcomes with the known characteristics of precipitation, we obtain an echo power estimator and a consistent censoring scheme, which allows us to operate at significantly lower effective levels of noise. The method aspects are validated with signals of sky, sun and precipitation, acquired by the WRM200 and WRK200 C-band dual-polarization radars, located in Kerava and Kumpula campus, Finland, surrounded by the Helsinki Test bed infrastructure.

In this approach, dual-polarization is an opportunity rather than a trade-off in detection capability. Dual-polarization has potential to diminish significantly the noise floor uncertainties, which limit the detectability of the power estimates from a single channel receiver. The initial loss of 3 dB can be recovered, and in fact, at will we gain further than that, to see more precipitation echo.

2. PRECIPITATION SIGNAL AND WHITE NOISE IN THE POLARIMETRIC SIGNAL COVARIANCE MATRIX

As known, the received complex signals projected in the horizontal (H) and vertical (V) polarizations of dual-polarization radar define the polarimetric signal covariance matrix ***R*** with expected values of

$$R \quad = < \begin{bmatrix} H \\ V \end{bmatrix} \begin{bmatrix} H & V \end{bmatrix}^* > = \begin{bmatrix} R_{hh} & R_{hv} \\ R_{hv}^* & R_{vv} \end{bmatrix} \qquad (1)$$

which can be taken as a generalization of the power measurement in single polarization $P_x = R_{xx} = |X|^2$, used for determination of radar reflectivity factor η_X, where *X* is *H* or *V.*

In conditions of low signal-to-noise ratio, the voltages compose of four significant terms: the horizontal signal *H* and the noise n_h, and the vertical signal *V* and the noise n_v. The noises are here taken uncorrelated and white. The expectation value of ***R*** then is

$$R = \begin{bmatrix} R_{hh}^S + P_h^N & R_{hv}^S \\ R_{hv}^{S*} & R_{vv}^S + P_v^N \end{bmatrix} \qquad (2)$$

We observe that the expectation value of the off-diagonal element is pure signal i.e. it is not affected by white noise. As known, the complex expectation value R_{hv} is zero for noise. In contrast, the legacy power estimators based on the diagonal terms are biased, unless subtracted for noise.

[1] *Corresponding author address:* Reino Keränen, Vaisala Oyj, P.O.Box 26, FI-00421 Helsinki, FINLAND; email: Reino.Keranen@vaisala.com

This leads us to consider the finitely sampled ray estimator

$$\left|\hat{R}_{hv}\right| = \frac{1}{M}\left|\sum_{i=0}^{M-1} H_i^* \, V_i\right| \qquad (3)$$

as a measure of the echo power, and subsequently of the radar reflectivity factors $\eta_{H,V}$. Noting $|\rho_{HV}(0)| \cong 1$ in precipitation, the off-diagonal element is linked with the diagonal terms through

$$\left|R_{hv}^S\right| \cong \sqrt{R_{hh}^S R_{vv}^S} \qquad (4)$$

Consequently, $\left|\hat{R}_{hv}\right|$ relates with the logarithmic mean of the reflectivity factors η_h and η_v, observed in a local interval at distance $\bar{r}$

$$\left|\hat{R}_{hv}(\bar{r})\right| \cong C_h (G_{dr})^{1/2} \; (\bar{\eta}_h \bar{\eta}_v)^{1/2} \Big/ \bar{r}^2 \qquad (5)$$

where C_h (and G_{dr}) are the radar system calibration constants of (differential) reflectivity. $\left|\hat{R}_{hv}(\bar{r})\right|$ can be summed through local range gates of weak precipitation, in which the differential phase Φ_{DP} keeps constant. Further in the mode of detection, we can use $\eta_h \approx \eta_v$ ($Z_{dr} = 0$). The legacy reflectivity then approximates as

$$\bar{\eta}_h \cong \left|\hat{R}_{hv}(\bar{r})\right| \times \frac{\bar{r}^2}{C_h (G_{dr})^{1/2}} \qquad (6)$$

The $\left|\hat{R}_{hv}(r)\right|$ based estimates are subject to the mean specific attenuation $(a_h(r) + a_v(r))/2$. Noticing that $\hat{R}_{hv}$ is readily computed for obtaining other polarimetric observables, we conclude that $\left|\hat{R}_{hv}(\bar{r})\right|$ is well-suited for real-time estimation of precipitation echo power, and hence a viable measure for radar reflectivity factor.

3. FEATURES OF $\left|\hat{R}_{hv}\right|$ FOR WHITE NOISE

The finitely sampled estimator $\left|\hat{R}_{hv}(\bar{r})\right|$ is a real positive-definite random variable. It is a function of samples of *M* complex voltages H_i and V_i, each consisting of Gaussian real and imaginary parts with zero mean. Both the precipitation signal and noise inputs follow the Rayleigh statistics.

In these conditions we consider the expectation value $P_{hv}'^{N} = <\left|\hat{R}_{hv}(\bar{q})\right|>_{|NOISE}$ and the variance $Var(P_{hv}'^{N})$ for white noise inputs. They quantify the degree of noise cancellation in finitely sampled rays. Through elementary integration, we obtain analytical expressions

$$P_{hv}'^{N} = \frac{\sqrt{n_h n_v}}{\sqrt{M}} \times \left\{\frac{\pi}{4} + \frac{M-1}{M}\left(1 - \frac{9}{8}\frac{\pi}{4}\right)\right\} \qquad (7)$$

$$Var(P_{hv}'^{N}) = \frac{n_h n_v}{M} \times \left\{1 - \left(P_{hv}'^{N\,2}\right)\right\} \qquad (8)$$

which at the limit of large *M* scale as

$$P_{hv}'^{N} \approx 0.902\sqrt{\frac{n_h n_v}{M}} \qquad (9)$$

$$Var(P_{hv}'^{N}) \approx 0.187\,\frac{n_h n_v}{M} \qquad (10)$$

The relations have been validated with the Kumpula radar data received in scans of cold sky and sun, an instance of which is displayed in Figure 1. Figures 2 and 3 display the functional dependencies on number of samples, accompanied with the data validation. These evaluations complement the calculations by Melnikov (2004).

We notice that the residual noise levels are low and obey the generic scaling law $\propto n_X / \sqrt{\mathrm{M}}$. In particular the variances are narrow. The features are promising measures of the degree of noise cancellation realized in finitely sampled rays. We note that the statistics of $P_{hv}'^{N}$ is not that of Rayleigh, for example the relation $Var(P) = <P>^2$ is not respected. We conclude that $P_{hv}'^{N}$ is sufficiently well-behaved, to be utilized with caution, for interpretations of the $\left|\hat{R}_{hv}\right|$ echo power at the limit of noise.

4. ENHANCED DETECTION CAPABILITY

In the conventions of Skolnik (1990), we study the expected detectability factors of $\left|\hat{R}_{hv}\right|$ in the realistic ranges of False Alarm Rates (FAR) and Probability of

Detection (POD), and compare the outcomes with the legacy power estimator $P_{h,v} = R_{hh,vv}$. For obtaining quantitative results, such as Figure 4, we apply a numerical model of Rayleigh signals and noise in two orthogonal channels. We generally reproduce the features of the legacy echo power estimation, as well as the analytical descriptions of the $\left|\hat{R}_{hv}\right|$ statistics. The model can be seen as a detailed description of the $\left|\hat{R}_{hv}\right|$ echo statistics, for combined inputs of precipitation signal and noise.

As a key aspect, we consider realistic uncertainties in the noise floor estimates. We study implications of semi static offsets, due slow variability in the noise floors caused by internal as well as external mechanisms, such as ground and atmospheric radiation. The noise floors have been reported to vary up to 2 dB from their nominal levels (cold sky samplings), due to external effects, see Seminario (2001). Effectively, we model simple scenarios of operation, in which the noise settings are not able to adapt, i.e. are kept constant, are evaluated too infrequently, or get updated with latency.

Typical sweep data contains 10^5-10^6 gates, implying FAR rates of 10^{-5} -10^{-6} deliver apparently high quality data. Use of state-of-the-art speckle filters brings this requirement down significantly, to the level of 10^{-2}, or below. The relative performances of the legacy power estimator and that of $\left|\hat{R}_{hv}(\bar{r})\right|$ turn out stable in such a span of FARs, at a fixed level of POD of 50%.

The main findings are, as visualized in Figure 4:

1. $\left|\hat{R}_{hv}(\bar{r})\right|$ offers a notable advantage over the legacy method in detectability in all the evaluated parameters settings - including the case of accurately known noise, for which the gain is at the level of 1-2 dB. This is consistent with the analyses in Ivic (2009).

2. The detectability factors of the $\hat{R}_{hh}$ based power estimator face a steep boundary, as soon as realistic variability of the noise floors is accounted for. This limits its detectability to a few dBs, typically, below the nominal noise floor, see Figure 4. Practically, there is no advantage in acquiring higher numbers of samples, despite the fact that in ideal conditions, such rays would deliver significantly narrower sampling fluctuations, and better detectability. The uncertainties of the noise means force safety margins to be applied in censoring. These outcomes agree with the common findings at operational radars.

3. The detectability of the $\left|\hat{R}_{hv}(\bar{r})\right|$ estimator is stable with respect to noise uncertainty. Because of this feature, the estimator has advantages of several dB with respect to the legacy estimator, as soon as realistic noise uncertainty is accounted for. The advantage is more significant for higher noise uncertainties, such as in intense rain. They grow very high, to the level of 10 dB, for maximal number of samples, available in range averaged ray data. These robust features are implied by the intrinsic noise cancellation in the off-diagonal matrix element.

5. $\left|\hat{R}_{hv}\right|$ AND CENSORED REFLECTIVITY FACTOR

The conversion of receiver signals into radar reflectivity can be described as steps of computation, in which the outcomes of the autocorrelation functions are expressed in units of signal-to-noise ratios. This serves for two purposes:

1. radar reflectivity calibration includes terms which factorize conveniently when applied to signal-to-noise ratios, and

2. signal-to-noise ratio suites well for censoring the gates in which noise dominates over the signal, to such a degree that the signal cannot be estimated. The objective of censoring is to be a practical fair realization of the optimal detectability factor, see Skolnik (1990), given the acceptable FAR and the prescribed POD.

The procedure, while straightforward in case of single channel signal (e.g. single polarization), easily looses its transparency as soon as one involves multiple channels and observations, each associated with varied levels of noise and detectability.

The simplicity of the $\left|\hat{R}_{hv}\right|$ estimator and the known characteristics of its residual noise allow realizing the conceptual detectabilty factors (see previous Section) as actual operational performances. In particular, user friendly censoring policies appear feasible such that equivalent image quality (equal FAR levels essentially) can be maintained between the signals obtained by the estimators $\left|\hat{R}_{hv}\right|$ and $\hat{R}_{hh}$ with few or no additional censoring parameters - with significantly better detection capability of the former approach, however.

6. EXAMPLES OF VALIDATION IN PRECIPITATION

We have computed reflectivity fields from data acquired at the Kerava radar, using a variety of echo power estimation methods ($\widehat{R}_{hh}$ and $\left|\hat{R}_{hv}\right|$ of total echo, as well as from clutter filtered spectra).

Figure 5 displays sweep data of Doppler filtered reflectivity, processed with operational settings typical in cool climates. Rays are comprised of 32 pulses. Two gates of 250 m are averaged in range. Both echo estimators, $\widehat{R}_{hh}$ and $\left|\hat{R}_{hv}\right|$, are censored for equal image quality, using SNR thresholds at the lowest feasible safety margin of 0.5 dB above the ideal level. At the ideal, both echo estimators would be censored for FAR at 6 10^{-6} after speckle filtering.

Qualitative comparisons can be made between the echo measured in the H-only mode ($\widehat{R}_{hh}$) and in the H+V mode ($\widehat{R}_{hh}$ and $\left|\hat{R}_{hv}\right|$ echo powers). One can distinguish the small impacts of the 3 dB lower transmitted power in the $\widehat{R}_{hh}$ echo data of the H+V mode. One can also see how the $\left|\hat{R}_{hv}\right|$ echo power recovers the sensitivity of the H+V mode back to the level of the H-only mode. It is to be noted that these processing settings are the most favorable to the legacy power estimator.

Additionally, $\left|\hat{R}_{hv}\right|$ echo data are displayed from the dedicated surveillance scan of rays with 128x16=2048. The coverage of continuous observations of precipitation is seen to expand by a few tens of kilometers, beyond the detectability range of the general purpose scans.

Figure 6 displays the uncensored and censored H+V sweep data acquired during large scale modest precipitation in warm season. The highest reflectivity values are at the level of 35 dBZ. Reflectivity fields of the methods of $\widehat{R}_{hh}$ and $\left|\hat{R}_{hv}\right|$ are reprocessed in rays of 64 pulses, with azimuth resolution of 0.5 degrees and no range averaging. In the uncensored sweep data, we observe the difference in the noise levels between the processings $\widehat{R}_{hh}$ and $\left|\hat{R}_{hv}\right|$. With censoring, both processings apply a SNR threshold at a very small safety margin of 0.4 dB above the ideal. The margin is adjusted for maximal performance of $\widehat{R}_{hh}$ in this sweep, in order to cross-check the censoring of $\left|\hat{R}_{hv}\right|$. At ideal settings both echo estimators would be censored for FAR 9 10^{-7}. No speckle filtering is applied, for clarity.

The sweep data of Figure 6 have been sampled into scatter plots of reflectivity versus range. These presentations, shown in Figure 7, allow for evaluations of the quality of censoring, and subsequently for determination of the minimally detectable signals, given the censoring applied. We find good data quality. We find the minimal detectable echo of $\widehat{R}_{hh}$ is at the level of 2.5 dB below SNR=1. The detectability of the $\left|\hat{R}_{hv}\right|$ method is further down by 2.8 dB. Both of these findings are in agreement with the expectations from the detection capability study. The safety margins applied here are deemed too low for cases of more intense rain, favoring the $\widehat{R}_{hh}$ estimator.

In Figures 8 and 9, the analyses shown in Figures 6 and 7 are repeated for processing settings which explore the limitations of the radar receiver, the signal processing and the echo power methodology: the autocorrelations are computed from 4096 samples summed from 16 consecutive gates of 256 ray pulses. No speckle filtering is applied. Uncensored data are displayed on top in Figure 8. We observe angular dependent noise floors in the $\widehat{R}_{hh}$ data, with enhanced noise levels in the directions of more intense rain. Two settings of censoring are tried, first at the safety margin of 0.6 dB above the ideal level, at which the echo estimators would censor for FAR at 6 10^{-5}. This setting is again deliberately tuned for optimal performance of $\widehat{R}_{hh}$. We find fair data quality in both processings, $\widehat{R}_{hh}$ and $\left|\hat{R}_{hv}\right|$. In contrast, an attempt to censor at a lower safety margin of 0.4 dB leads to appearance of significant noise speckle, which seems associated with elevated noise levels in rays with significant rain spanning more than 100 km in range.

In Figure 9 data, the minimal detectable signal of the $\widehat{R}_{hh}$ estimator determined to the level of 7 dB below the level SNR=1, while the detectability level of $\left|\hat{R}_{hv}\right|$ is further down by 7 dB. These outcomes agree with our expectations - however the setting is again deemed too fragile in a general weather case. At fair safety margins of 1 and 2 dB, the relative advantages of $\left|\hat{R}_{hv}\right|$ are close to 10 and 11 dB, respectively.

Most important, we find out that the radar system, the measurement of echo power in particular, performs largely as expected up to these extreme processing settings, configurable in the standard signal processing. It is remarkable that precipitation echoes are observed at signal-to-noise ratios far below 10 dB, while still maintaining a decent image quality (FAR).

Figure 10 is a simple study into gate level differences in the reflectivity fields obtained with $\widehat{R}_{hh}$ and $\left|\hat{R}_{hv}\right|$. We divide the sweep data shown in Figure 6 in two subsets. The data at radii less than 90 km are evidently of non-meteorological origin, while the distinct subset of data at radii more than 90 km are likely precipitation. We find the $\widehat{R}_{hh}$ and $\left|\hat{R}_{hv}\right|$ based reflectivity values are highly correlated in precipitation, with a mean difference less than 0.5 dB, which can be taken as a first estimate of typical bias in these two observations.

Figure 11 illustrates impacts of the enhanced detection capability of the $\left|\hat{R}_{hv}\right|$ based echo power estimation in a case of far distance large scale precipitation, approaching the Kerava radar from west. The composite product from the NordRad network of the regional national meteorological services is used as a reference. The example suggests that observing reflectivity fields obtained from the $\left|\hat{R}_{hv}\right|$ based echo power, and by using scan settings dedicated for far distance detection, one can unambiguously observe the large scale weather system about an hour earlier than with the legacy method.

7. CONCLUSIONS

We have explored the basic properties of the polarimetric signal covariance matrix for the task of detecting weak echo of precipitation. We have constructed and initially evaluated methodology which enhances the capability of the dual-polarization weather radar to detect weak precipitation echoes.

The enhancement is based on noise cancellation that occurs in the off-diagonal element R_{hv} , which allows suppressing the uncertainties in the noise subtraction applied to the legacy power estimator.

In typical operational processing settings, the enhancement compensates the 3 dB loss of sensitivity due to split transmitter power. The enhancement factor grows rapidly as function of number of independent samples, as well as for higher safety margins of censoring, necessary in conditions of variable external noises e.g. intense rain.

8. ACKNOWLEDGEMENTS

The study is part of the research conducted within the FiDiPro professorship program by the Finnish Funding Agency for Technology and Innovation.

9. REFERENCES

Ivic, I.R., Zrnic D.S., Tian Y., 2009: "The Use of Coherency to Improve Signal Detection in Dual-Polarization Weather Radars", J. of Atm. and Oc.Tech. **26**, 2474-2487;

Ivić I.R., Melnikov V.M., 2011: "Enhancing Signal Detection in dual-polarization weather radars by combining the coherency based detection with 2D despeckling", 35th Conference on Radar Meteorology;

Keränen R. Chandrasekar V., 2011 "Off-diagonal Element Echo Power Estimator for Polarization Weather Radar" U.S./PCT/DE Patent Application;

Melnikov V.M., 2004 "Simultaneous Transmission Mode for the Polarimetric WSR-88D; Statistical Biases and Standard Deviations of Polarimetric Variables" CIMMS Report, June 2004;

Seminario M., Gojara K. and Chandrasekar V., 2001: "Noise Correction of Polarimetric Radar Measurements" 30th Conference on Radar Meteorology;

Skolnik M. ed., 1990: "Radar Handbook" 2nd edition, McGraw-Hill.

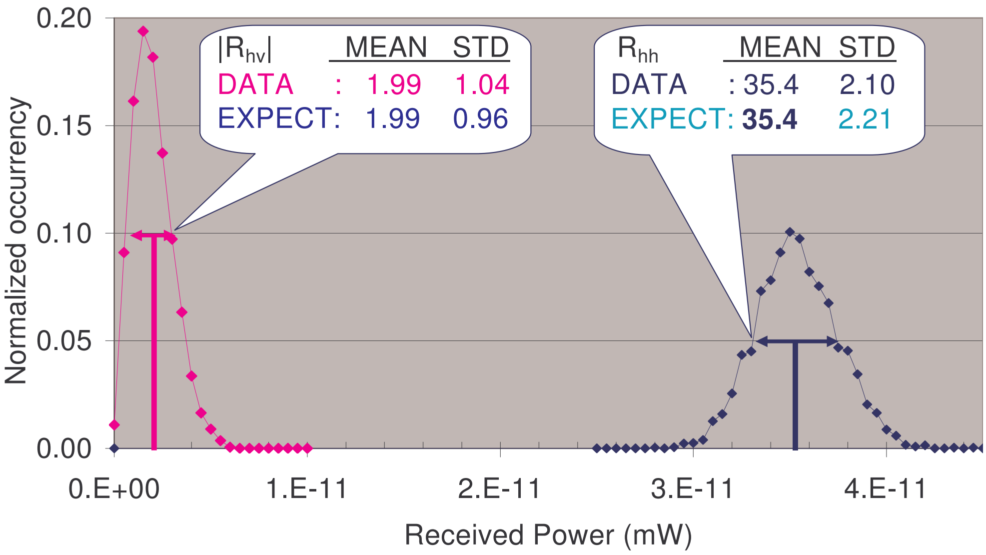

Figure 1. Distributions of the received power from Sun signals, as estimated by $|R_{hv}|$ and R_{hh}, computed in rays of 256 samples at the Kumpula radar.

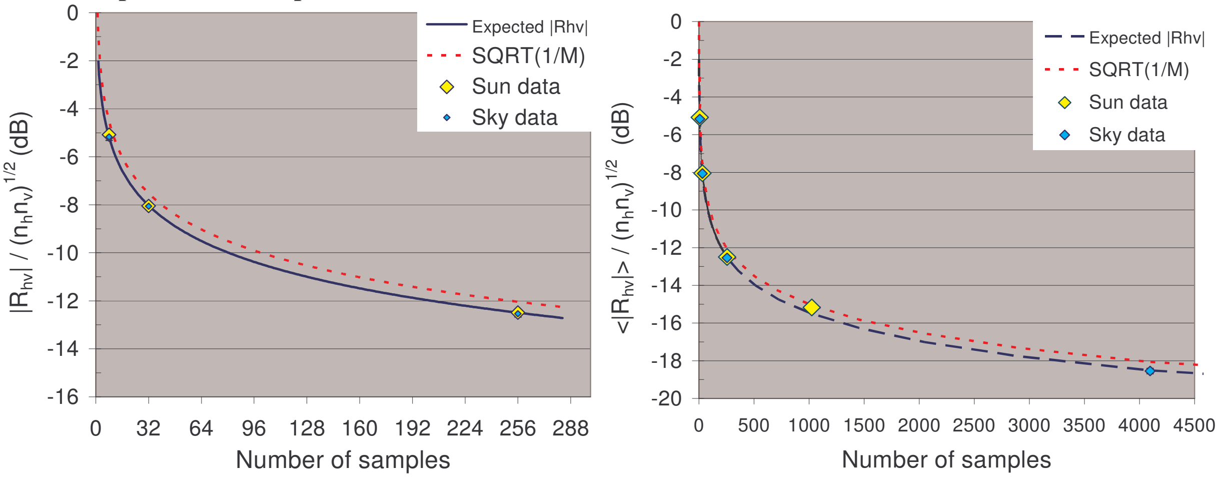

Figure 2. The trend of the expected mean of the residual noise floor in $|R_{hv}|$ (blue line) as function of number of independent samples (two spans displayed), normalized to the geometric mean of the noise levels in the H and V channels. The dotted red line is a generic scaling of $1/(n_h n_v)^{1/2}$. The symbols represent measurement data acquired in the sun and cold sky scans by the Kumpula radar.

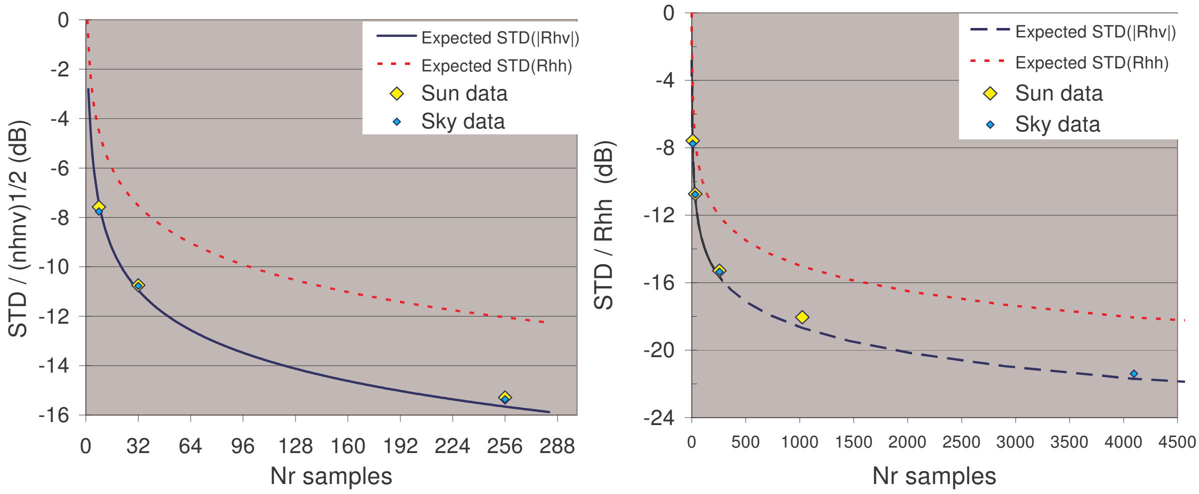

Figure 3. The trend of the expected standard deviation of the residual noise floor in $|R_{hv}|$ (blue line) as function of number of independent samples (two spans displayed), normalized to the geometric mean of the noise levels in the H and V channels. The dotted red line is the scaling of $STD(R_{hh}) = (n_h n_v/M)^{1/2}$. The symbols represent measured standard deviations, in the data acquired from sun and cold sky scans by the Kumpula radar.

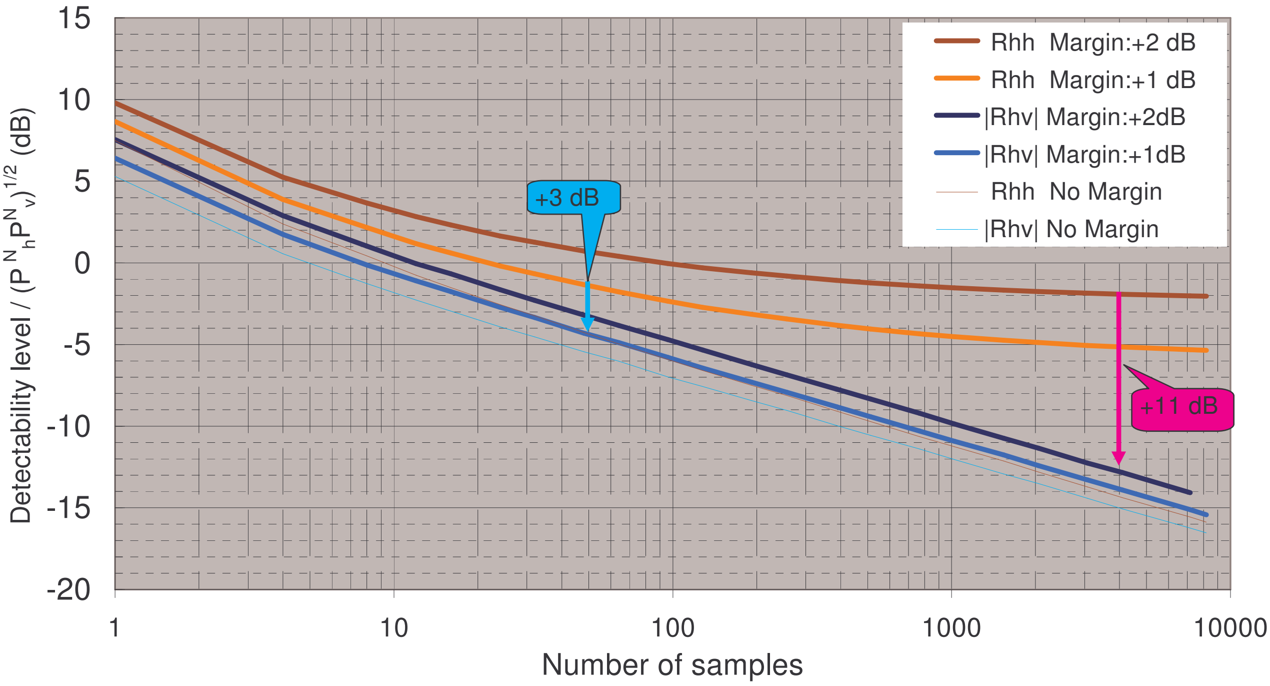

Figure 4. Detection capabilities of the echo power estimators $|R_{hv}|$ and R_{hh} as function of number of independent samples, in the conventions of Skolnik (1990). The curves are computed at the false alarm rate of 0.01, and at 50% probability of detection, providing high quality data when noise speckle filters are used. The blue shaded curves are for the $|R_{hv}|$ estimator with no safety margin in SNR censoring (thin light blue line), with censoring at a margin of 1 dB (blue), and with censoring at 2 dB margin (dark blue) of uncertainty in the mean noise floors (thick line). The brown lines are the corresponding expectations for the R_{hh} power estimator, at vanishing safety margin, and at margins of 1 and 2 dB, respectively. The arrows and the legends visualize the advantages of the $|R_{hv}|$ estimator over R_{hh} at samplings of 50 at 1 dB safety margin (light blue) and at sampling of 4096 at the margin of 2 dB (pink).

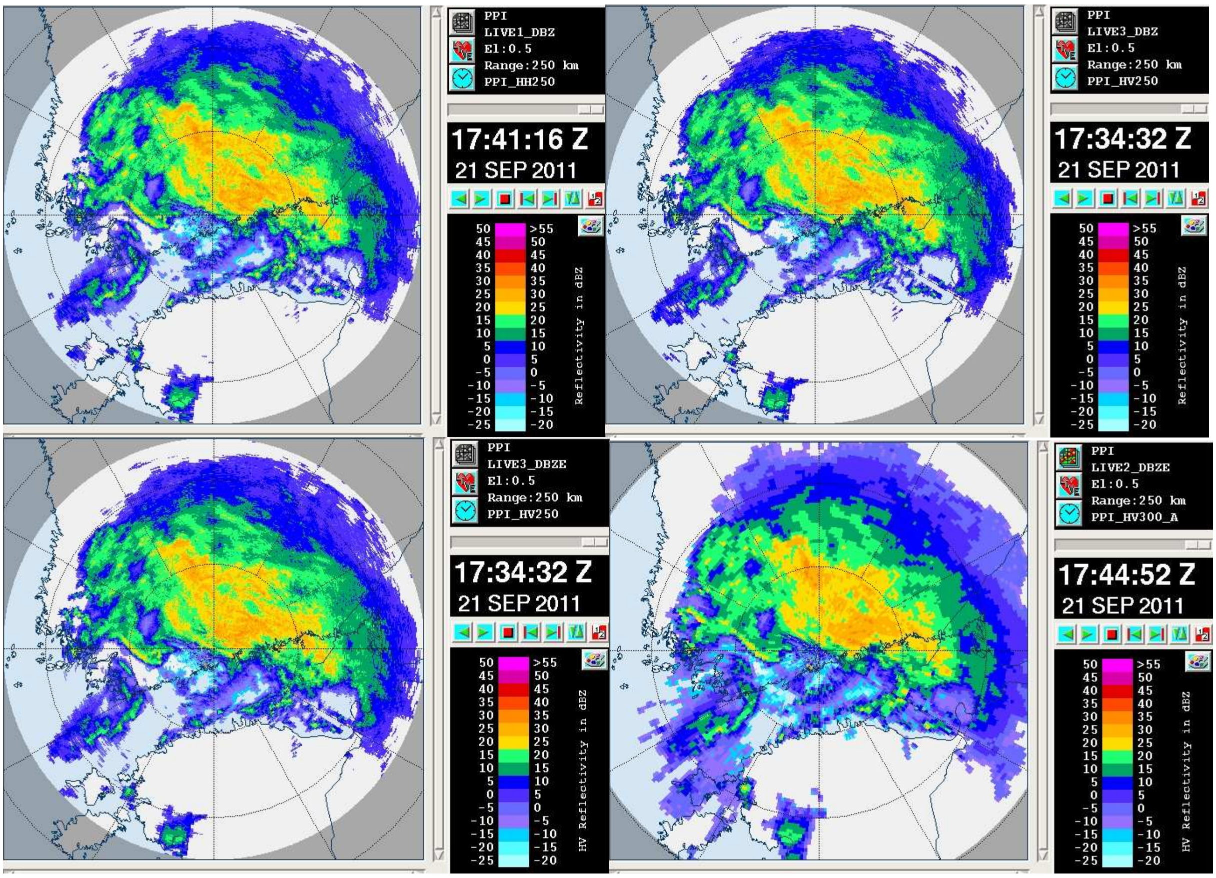

Figure 5. Displays of Doppler filtered reflectivity fields in large scale precipitation, acquired with various modes of processing at the Kerava radar, in a time span of ten minutes. Top left data are R_{hh} echo power in the H-only mode; top right data are R_{hh} echo power in the H+V mode; bottom left data are $|R_{hv}|$ echo power in the H+V mode. All these three sets of data are rays of 32 pulses. The moments are averaged over two gates in range. The bottom right data are $|R_{hv}|$ echo power in the H+V mode, acquired in a scan optimized for far distance echo (moments from 128 pulses in rays with averaging over 16 consecutive gates).

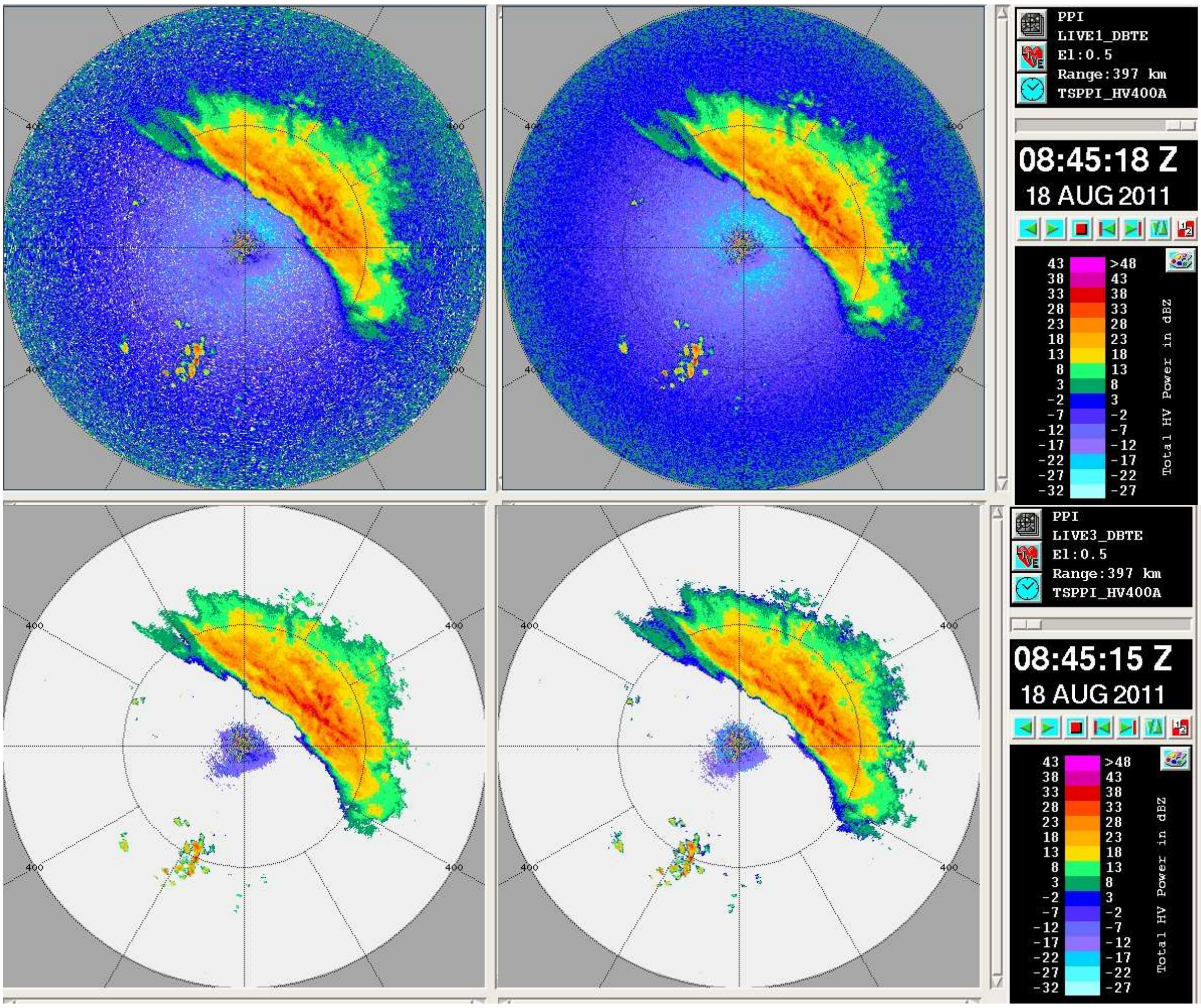

Figure 6. Sweeps of data from large scale precipitation acquired by the Kerava radar, reprocessed with varied methods of power estimation and varied levels of censoring, *M=64*. The top row are computed with no sensoring, while in the bottom row, data are censored with a small safety margin of 0.4 dB. In the left column, data are from the R_{hh} estimator. In the right column, data are from the $|R_{hv}|$ estimator. For other processing settings, see the text. See Figure 7, for detailed comparison of detectability.

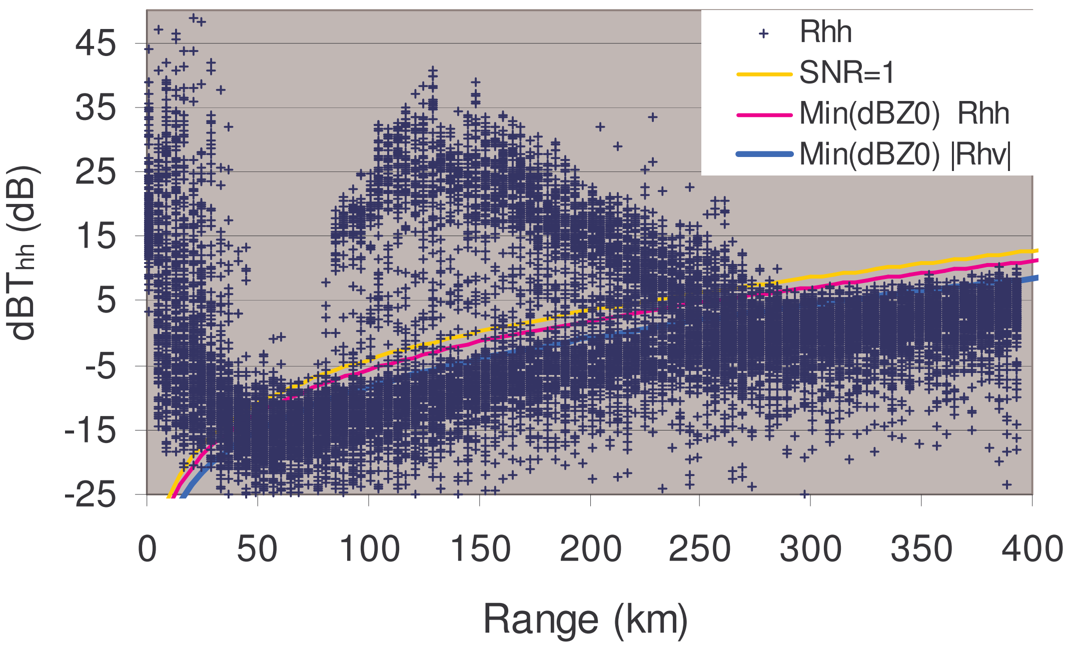

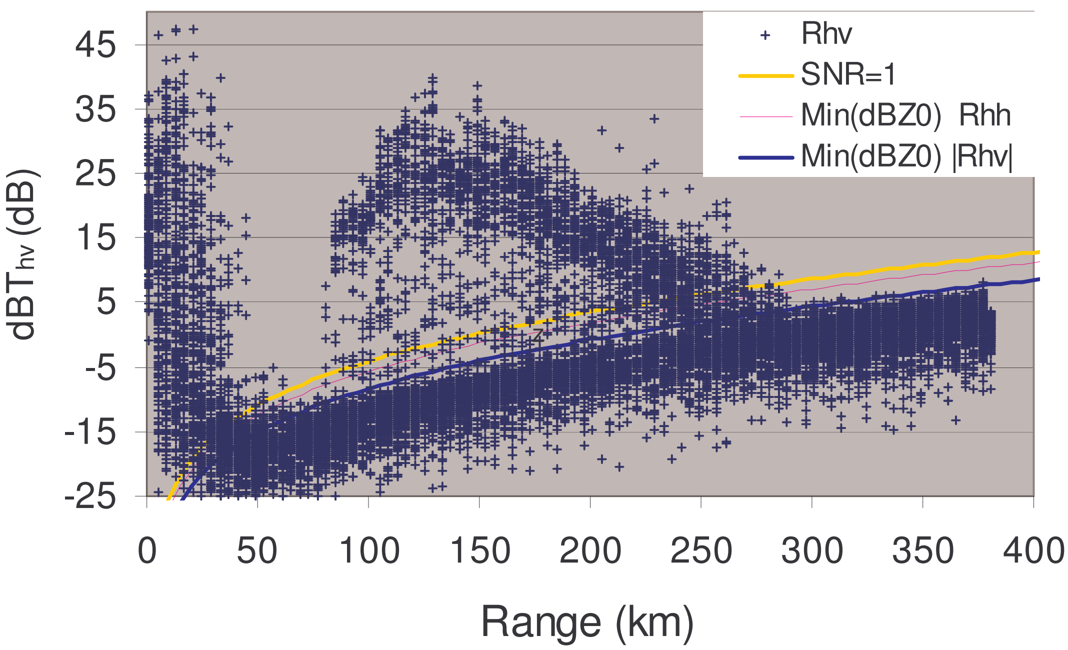

Figure 7. Sampled sweep data, from Figure 6, projected in the scatter plots of reflectivity from R_{hh} (top), and from $|R_{hv}|$ (bottom) as function of range. The yellow line represents the levels of reflectivity at SNR_{hh}=1 (corresponding to minimal dBZ_h of -5.8 dBZ at distance of 100 km), the red curve defines censoring of R_{hh} at safety margin of 0.4 dB (corresponding to minimal dBZ_h of -7.3 dBZ at the distance of 100 km), and the blue curve is defnes the equivalent censoring of the $|R_{hv}|$ echo (corresponding to the minimal detectable signal of dBZ_{hv} of -10.0 dBZ at 100 km distance.

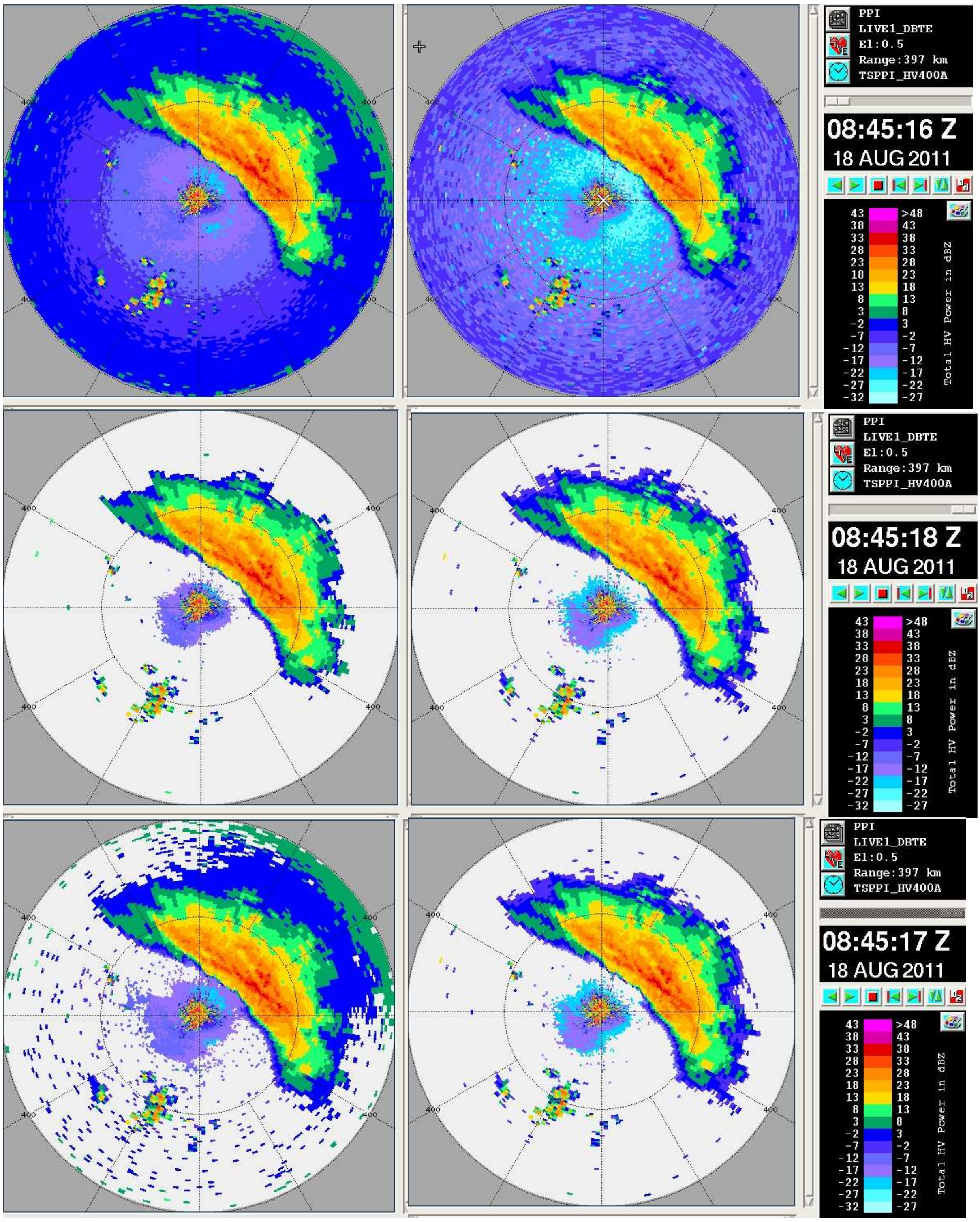

Figure 8. High sampling data from large scale precipitation acquired by the Kerava radar, with varied methods of power estimation and varied levels of censoring. Top row are uncensored data. The middle row data are censored using a SNR threshold with margin of 0.6 dB, adjusted to this particular R_{hh} data set, while the bottom row is a failed attempt to censor at the margin of 0.3 dB. On the left, the data are from the R_{hh} estimator. On the right, the data are from the $|R_{hv}|$ estimator. See Figure 9 for detailed comparison of detectability.

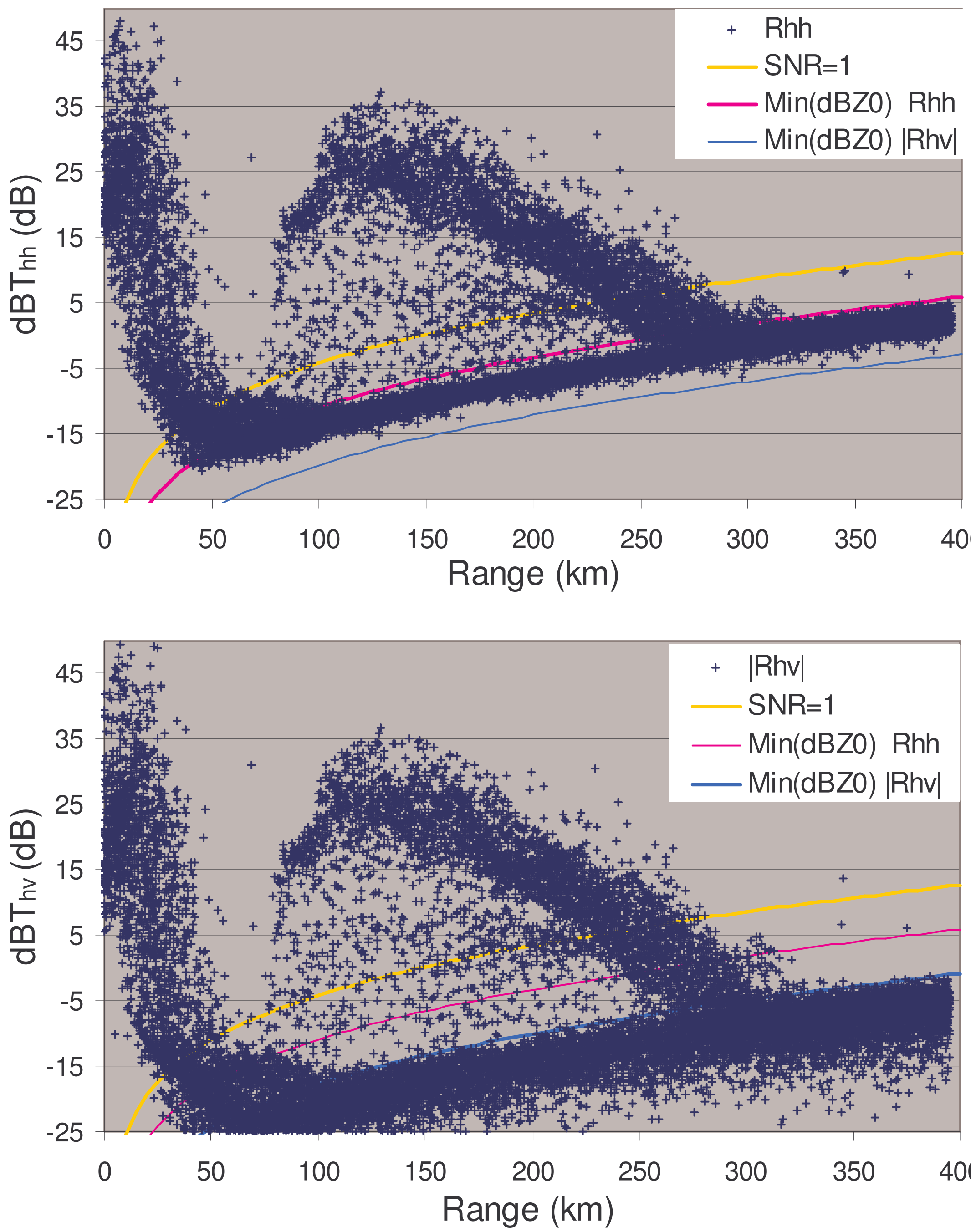

Figure 9. The sweep data, displayed in Figure 8, projected in the scatter plot of reflectivity from R_{hh} (top), and from R_{hv} (bottom) as function of range. The yellow line represents the levels of reflectivity, at SNR_{hh}=1 (corresponding to minimal dBZ_h of -5.8 dBZ at distance of 100 km), the red curve is defined by the censoring on SNR_{hh} at the safety margin of 0.6 dB (corresponding to minimal dBZ_h of -12.5 dBZ at the distance of 100 km), and the blue curve is an outcome of the equivalent censoring on $|R_{hv}|$ (corresponding to the minimal detectable signal of dBZ_{hv} of -19.2 dBZ at 100 km distance).

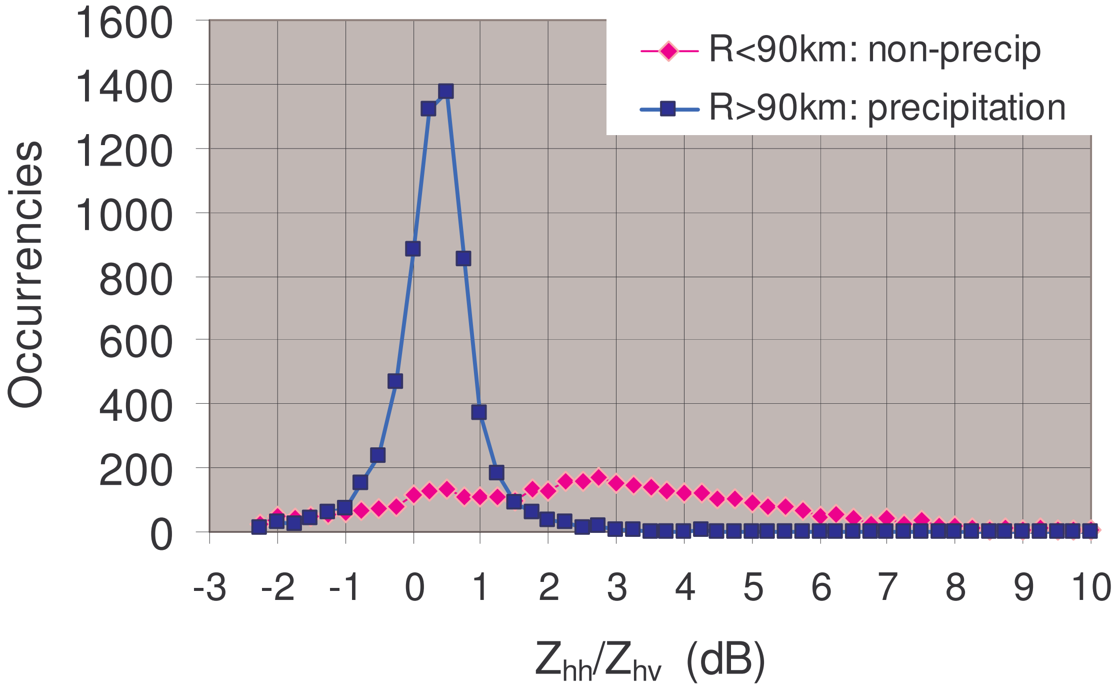

Figure 10. Distribution of the gate-by-gate ratios of the Doppler filtered reflectivity obtained from the R_{hh} echo power estimator and the $|R_{hv}|$ echo power estimator. The observations are from the sweep data shown in Figure 6, divided in two subsets. The pink histogram consists of data at radii less than 90 km, which are evidently of non-meteorological origin. The blue histogram consists of gate data at radii more than 90 km, apparent precipitation.

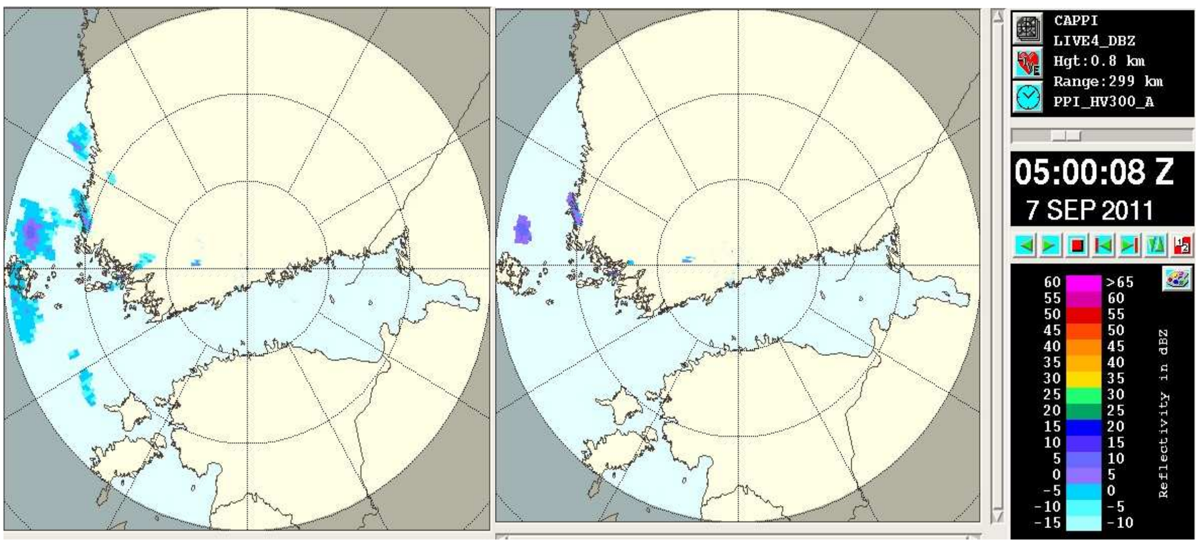

Figure 11. A weather case visualizing the impact of the enhanced echo detection capability of the $|R_{hv}|$ based echo estimation. On top left, the display of $|R_{hv}|$ based reflectivity field (PPI at elevation of 0.5 degrees) which allows for unambiguous detection of the large scale precipitation approaching from west. On top right, the observations of the legacy power estimator for comparison. Bottom: the composite product of the NordRad radar network (05 UT, constant altitude PPI) validating the observation of precipitation (source: the Finnish Meteorological Institute, public service at http://ilmatieteenlaitos.fi/sade-pohjoismaat.